JOURNAL OF OPTOELECTRONICS AND ADVANCED MATERIALS Vol. 9, No. 5, May 2007, p. 1206 - 1214

Section 1. Growth and characterization of inorganic crystals
Invited Paper

A new generation of nonlinear optical and laser crystals of rare earth borate and tantalate families

N. I. LEONYUK, E. CAVALLI[a], G. CALESTANI[a], N.V. KULESHOV[b], J.M. DAWES[c],
V.V. MALTSEV, E.V. KOPORULINA, E.A. VOLKOVA, O.V. PILIPENKO
Department of Crystallography, Moscow State University, Moscow, Russia
[a]Dipartimento di Chimica Generale ed Inorganica, Chimica Analitica e Chimica Fisica, Università di Parma, Parma, Italy
[b]Insitute for Optical Materials and Technologuies, BNTU, Minsk, Belarus
[c]Centre for Lasers and Applications, Macquarie University, NSW 2109, Australia

RE:$YAl_3(BO_3)_4$ (*RE* = Yb, Er) and *RE*Ta_7O_{19} (*RE* = Y, Nd, La) single crystals have been obtained using $K_2Mo_3O_{10}$ based flux by spontaneous nucleation as well as dipping seeded high-temperature solution growth. Their composition and physical characteristics were compared in light of the growth conditions. It was found that the average *RE* segregation coefficients vary from 0.80 to 1.02. The spectroscopic and stimulated emission properties of (Er,Yb):$YAl_3(BO_3)_4$ crystals have been investigated and efficient continuous-wave (CW) and Q-switched pulsed laser operation under diode pumping have been demonstrated. The absorption and emission spectra of Nd^{3+}:YTa_7O_{19} (Nd:YHT), and Nd^{3+}:$LaTa_7O_{19}$ were measured at 10 and 300 K. The absorption and emission spectra of Nd:YHT, and $NdTa_7O_{19}$ were studied at 10 and 300 K and are discussed on the basis of the structural data. The room temperature spectra show a marked inhomogeneous broadening that makes these crystals promising for tunable solid-state laser applications

(Received November 14, 2006, after revision March 3, 2007; accepted April 12, 2007)

Keywords: Rare earth borates, Tantalates, Flux crystal growth, Diode-pumped lasers, Q-switched lasers, Absorption spectra, Emission spectra, Non-radiative processes

1. Introduction

From the viewpoint of crystal chemistry, there are numerous structural types of technologically promising borates due to their tendency to form various complex polyanions. Of them, the rare earth (*RE*) borate family is very popular, especially, considering the wide isomorphous substitutions in *RE* positions. Recently attention is focused on polyfunctional non-centrosymmetric huntite type orthoborates *RE*$Al_3(BO_3)_4$ (*RE*AB) which are of great interest as promising solids for lasing and non-linear optical applications. For example, Yb and Tm doped $YAl_3(BO_3)_4$ (YAB) self-frequency-doubled laser crystals can offer the prospect of broad tunability in the infrared and visible, and operate at high pump powers with minimal thermal effects [1-3].

On the other hand, lasers emitting at 1.5 μm are very attractive for several industrial applications in range-finding, environmental sensing, telecommunications, surgery, etc. This is first of all due to the eye-safety of 1.5-μm radiation. Other advantages of this wavelength are its high transparency in atmosphere and fused-silica waveguides, and the availability of sensitive room-temperature light detectors (Ge and InGaAs photodiodes). These conditions are mostly fulfilled by Er,Yb-codoped phosphate glasses, but glasses suffer from poor thermal and mechanical stability which limits the laser power to the level of few hundreds miliwatts due to thermal lensing effects and optical damage of the active element. Thus (Er,Yb)-codoped crystalline matrices are still intensively investigated. Room-temperature 1.5 μm lasing has been obtained in (Er,Yb)-doped $Y_3Al_5O_{12}$ [4], $Ca_2Al_2SiO_7$ [5], Er-doped $LaBO_3$, $GdBO_3$ [6], Er:YVO_4 [7]. The most efficient diode-pumped laser action to date has been demonstrated in (Yb,Er)-doped oxoborates. In $Ca_4GdO(BO_3)_3$, output power of about 80 mW was demonstrated with slope efficiency of 7% [8]. Most of the *RE*AB crystallize, as a rule, in R32 space group (i.e. huntite type symmetry), but Nd-, Gd-, Sm-, Eu- and Pr-representatives also have high temperature monoclinic modifications, C2/c and C2 space group with phase transitions at 880-900 ^oC, 1040-1050 ^oC, 1130-1150 ^oC, 1130-1150 ^oC and 1080 ^oC respectively [9].

Another group of prospective materials is the rare earth (*RE*) heptatantalates *RE*Ta_7O_{19} family (*RE*HT) [10,11]. Polycrystalline solid solutions $(Nd_x,La_{1-x})Ta_7O_{19}$ have been shown to be of interest in luminescence and laser applications [12]. Single crystals of these compounds possess good thermal and chemical stability, allowing a high neodymium concentration, with good luminescence properties. In particular, $NdTa_7O_{19}$ (NHT) is characterised by a relatively low efficiency of the non-radiative processes [13]. These properties make them and the heptatantalates in general, attractive media for solid-state

laser technology. Moreover, recent X-ray diffraction (XRD) investigations for the *RE*Ta_7O_{19} (*RE* = La-Nd) series have indicated that these crystals belong to the $P\bar{6}c2$ space group [14] with some preference for the latter. This non-centrosymmetric space group is compatible with the non-linear optical properties of the host matrix, and this could extend the potential applications of these materials.

Despite a number of publications on crystal growth and characterization of these compounds, there are no systematic investigations of their composition, homogeneity, morphology and structural characteristics depending on the flux growth conditions. In the present work, we consider the systems (*RE*,Y)$Al_3(BO_3)_4$, (*RE*YAB) where *RE* = Er and Yb, *RE*HT (*RE* = Y, La, Nd) and mixed Nd^{3+}:YTa_7O_{19} (Nd:YHT) , and Nd^{3+}:$LaTa_7O_{19}$ (Nd:LHT) from this point of view. Also, an attempt is made to obtain Yb:YAB epitaxial layers as a first step towards their growth technology. Some structural refinement of *RE*HT crystals has been done. Moreover, recent results on spectroscopic and laser characteristics of these materials are presented. Since crystal twins are known to occur in many crystals, a valuable technique for characterising the nonlinear performance of the crystal to identify the presence of twins in these materials has been developed.

2. Experimental

2.1. Crystal growth, composition and structure

The choice of solvent is a major concern for successful flux growth experiments. *RE*Al huntite borates tend to decompose, in part, into *RE*BO_3 and the aluminium aluminoborate having two-dimensional polyanion $Al_3BO_9^{6-}$ in which AlO_4 tetrahedra and BO_3 triangles are joined by sharing common corner O atoms [9]. This mixed polyanion with four-fold coordinated Al atoms has a rather high thermodynamic stability at enhanced temperatures. For this reason, the growth technology of *RE*AB crystals is based on potassium trimolybdate fluxes. A motivation is low melting temperatures, high chemical activity and dissolving ability of alkali polymolybdate melts. With respect to Ref. [9], an addition of B_2O_3 increases the solubility of $K_2Mo_3O_{10}$ solutions, and it results in decreasing saturation temperature. Furthermore, the volatility of such flux would be reduced without a substantial distinction in its viscosity. For the same reasons, potassium trimolybdate $K_2Mo_3O_{10}$ with an excess of boron oxide can be considered as a possible solvent in the case of *RE*HT as well.

The crystals $RE_xY_{1-x}Al_3(BO_3)_4$, with x = 0.07 to 0.15 (*RE* = Yb) and x = 0.005 to 0.01 (*RE* = Er) in the starting crystalline substances were grown by dipping seeded high-temperature solution growth (DSHTSG) using $K_2Mo_3O_{10}$ based fluxes. Concentrations of Yb and Er doped YAB in the initial load were 20 wt% and 17 wt.%. According to Ref. [9], the field of YAB primary crystallization in the system YAB-($K_2Mo_3O_{10}$-B_2O_3-Y_2O_3) has wider temperature-concentration boundaries at 17 wt% in comparison with 20 wt.%. Consequently, this flux composition is more acceptable for growth of slightly doped YAB crystals. Starting chemicals (not lower than 3N purity in all runs) were as Y_2O_3, Yb_2O_3, Al_2O_3 and B_2O_3, but $K_2Mo_3O_{10}$ was previously sintered from K_2MoO_4 and H_2MoO_4 at 650°C according to the scheme:

$$K_2MoO_4 + 2H_2MoO_3 = K_2Mo_3O_{10} + H_2O\uparrow.$$

Before DSHTSG, saturation temperatures of the fluxed melts were precisely determined by a probe technique, and the supersaturation was kept within certain limits by the cooling of fluxed melts in the range of 0.2-5°C/day following to the experimental data on the solubility and the crystallization kinetics. The epitaxial layers of Yb:YAB with 5 and 10 at% of Yb and YAB substrates were obtained in the same systems.

In the case of *RE*HT an additional investigation of the phase formation was made. Thus, compositions of initial mixture in *RE*HT crystal growth experiments were chosen within the fixed regions of *RE*HT primary crystallization. RE_2O_3/Ta_2O_5 ratio corresponded to the stoichiometry in the chemical formula of the heptatantalate. The molar ratio of $K_2Mo_3O_{10}/B_2O_3$ was varied from 1:1 to 10:1. The starting charges were placed into platinum crucibles and homogenised at 1150-1200°C in high-temperature furnace for 6-24 hours. Then, the temperature was lowered to 900-950°C at a rate of 1.5-0.5°C/h. Finally, the fluxed melt was quickly cooled down to 300°C, and the crucibles were moved out from the furnace.

The composition, homogeneity and external morphology of grown crystals were studied by the analytical scanning electron microscope (ASEM) JSM-5300 + Link ISIS. Electron microprobe analysis (EMPA) of polishing samples was performed with an accuracy of 0.2-0.3 wt %. A Cameca analyzer was used for study of crystals with a minor dopant concentration. In this case, the accuracy has been increased up to 0.02-0.03 wt.%.

The segregation coefficients (*K*) of were calculated basing on the following equation $K=C_{cryst}/C_{diss\ REYAB\ (REHT)}$, where C_{cryst} is *RE* content in grown crystals and C_{diss}. *REYAB (REHT)* is *RE* concentrations in the corresponding crystalline substances of the fluxed melt.

X-ray powder diffraction patterns of solids were obtained by using the CuK_α radiation with a Thermo X'tra powder diffractometer. Single crystal diffraction data were collected with a Bruker SMART CCD diffractometer equipped with MoK_α radiation. Structure refinement was performed with SHELX97 [15].

2.2. Spectroscopy

The absorption spectra of the borate crystals were measured using a Cary-500 spectrophotometer with spectral resolution of 0.4 nm. As an excitation source for lifetime measurements the optical parametric oscillator LOTIS LT-2214OPO pumped by Nd:YAG laser was used. The stimulated emission cross section spectra were calculated by using reciprocity method:

$$\sigma_{em}(\nu)=\sigma_{abs}(\nu)\cdot\frac{Z_g}{Z_e}\cdot\exp[(E_{ZL}-h\cdot\nu)/kT],$$

were Z_g and Z_e are the partition functions of the ground state (g) and excited state (e), E_{ZL} is the energy of the zero line (energy gap between the lowest Stark components of each manifold), $\sigma_{abs}=\alpha/N$ is the ground state absorption cross section, α is an absorption coefficient, N is an Er^{3+} ions concentration.

The absorption and emission spectra and the fluorescence decay times of *RE*HT were measured in the 400-1150 nm range using a spectroscopic setup described in a previous paper [13]. In this case, however, the emission spectra have been obtained in the 850-1150 nm region after excitation at 514 nm (Ar^+ laser).

2.3. Nonlinear and laser experiments

Since the quality of nonlinear laser crystals depends on the refractive index variation and active ion density, this latter feature is studied by the technique suggested for the first time in [16]. By illuminating the full crystal face with a high peak power laser beam, and then observing the second harmonic signal on a charge coupled device camera using bandpass filters, it is possible to quantify the nonlinear performance of the crystal across its face and to identify the presence of twins in one series of non-destructive measurements as the crystal orientation is adjusted. The self-doubled green laser output experiment for *RE*YAB crystals was measured by using a 3×3×3 mm sample of crystal cut for type I phase matching (ϕ=0°, θ=31°). The pumping source was an InGaAs LD with the peak emission wavelength at 975 nm. The CW (Er,Yb):YAB laser experiments were carried out with a nearly hemispherical cavity consisting of 50-mm radius-of-curvature output coupler and plane high reflector mirror. A CW fiber-coupled (∅=100 μm, N.A.=0.22) laser diode with maximum output power of 5.5 W emitting near 980 nm was used as a pump source. The 1.5-mm-thick laser element was mounted on a copper heatsink (without active cooling) inside the resonator close to the plane high reflector mirror. The cavity-mode diameter at the active element was close to the pump beam waist. The Q-switching measurements were performed with the same cavity configuration. As a passive shutter 110-μm-thick Co^{2+}:$MgAl_2O_4$ crystal with initial transmission of about 99.5% at 1604 nm was used.

Using *RE*HT crystals, the benchmark second–harmonic generation (SHG) test performed using a pulse Nd:YAG laser in the reflection mode [17] attested to a noncentrosymmetrical structure of the LHT crystals.

3. Results and discussion

3.1 Crystal growth, composition and structure

Visually transparent *RE*YAB crystals were obtained with a typical size up to 10×10×15 mm^3 (Fig. 1). All single crystals for this borate family have a characteristic set of simple crystallographic forms: two trigonal prisms {11 $\bar{2}$0}, {2 $\bar{1}$ $\bar{1}$0} and rombohedron {10 $\bar{1}$1}, differently developed depending on the type of doping cations and growth conditions. *RE*YAB crystals (RE = Yb) are colorless, but the Er:YAB samples have the characteristic "erbium" light-pink colour.

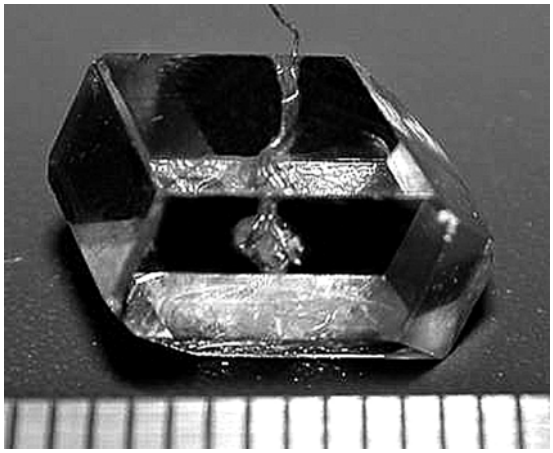

Fig. 1. Typical REYAB crystals grown by DSHTSG method.

It was found that the average Er and Yb segregation coefficients vary from 0.80 to 1.02, as a consequence of minor differences in the sizes of Y^{3+} and RE^{3+} cations.

The growth rates of the Yb:YAB crystal layers were estimated to be within the range of 0.07-0.61 μm/mm. These values are higher in comparison with the growth rate of the $NdAl_3(BO_3)_4$ epilayers obtained from PbO-PbF_2 based flux system on the $Gd_{0.59}La_{0.41}Al_3(BO_3)_4$ [18]. On the other hand, experimental data of this work agree with earlier results on YAB bulk crystal growth from $K_2Mo_3O_{10}$ based high temperature solutions [9]. From the ASEM data, it was found that Yb concentration in grown films slightly increases from 0.09 to 0.11 at ytterbium position with an increase of supersaturation, but these variations are not dramatic at this stage.

The NHT crystal morphology greatly depends on the growth conditions, first of all, on the $K_2Mo_3O_{10}/B_2O_3$ ratio in the fluxed melt. An increase in the concentration of $K_2Mo_3O_{10}$ in the complex solvent promotes the development of pinacoidal faces {0001}(Fig. 2*a*-*c*). The same tendency was also observed for the Y – representative of these heptatantalates. Only plate-like YHT crystals were found when the initial solvent was enriched in $K_2Mo_3O_{10}$. Since the $K_2Mo_3O_{10}$ concentration decreased, the {10 $\bar{1}$0} and {11 $\bar{2}$0} simple forms prevailed over the pinacoid face and isometric crystals crystallized with plate-like shape. In comparison with the neodymium system, no elongated crystals were found. A possible reason for this effect is a decreasing of the *RE*–O distance in the $RETa_7O_{19}$ structure, taking into account different ionic radii of Y^{3+} and Nd^{3+} (0.900 Å and 0.983 Å, respectively), which leads to decreasing in the unit–cell volumes of the yttrium (661.96 $Å^3$) and neodymium (669.29 $Å^3$) analogues. Thus, the surface energy of

different faces and, respectively, crystal morphology depends on the type and size of *RE* cation.

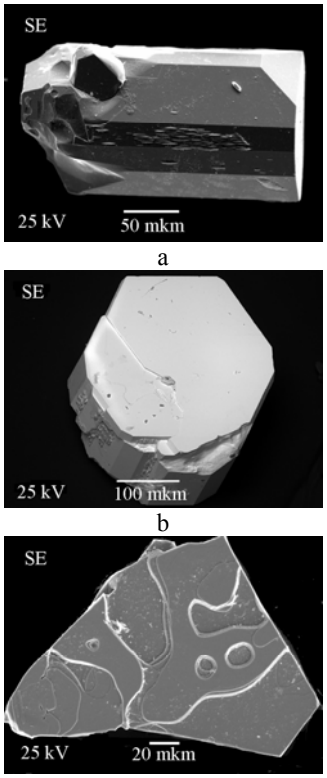

Fig. 2. Different type of NHT crystals: a) an elongate (solvent: 50 wt% $K_2Mo_3O_{10}$ - 50 wt% B_2O_3), b) an isometric (solvent: 75 wt% $K_2Mo_3O_{10}$ - 25 wt% B_2O_3), c) plate-like (solvent: 90.91 wt% $K_2Mo_3O_{10}$ - 10.09 wt% B_2O_3).

A comparison of unit cell parameters of NHT, Nd:YHT and Nd:LHT crystals calculated from X-ray powder diffraction data is reported in Table 1.

Table 1. Unit cell parameters of hexagonal NHT, Nd:YHT and Nd:LHT crystals

Compounds	a, Å	c, Å	V, Å^3
NHT	6.225(2)	19.94(2)	669.29(1)
Nd:YHT	6.203(2)	19.86(2)	661.96(1)
Nd:LHT	6.238(2)	19.995(18)	669.29(1)

The crystal structure of Nd:LHT was determined. The results of this analysis are summarized in Tables 2 and 3. Structure refinement, performed with confirmed that Nd:LHT crystallizes in the non-centrosymmetric space group $P\bar{6}c2$. The structure (Fig. 4) consists of double layers of pentagonal TaO_7 bipyramids developing perpendicularly to the *c* axis, intercalated by a layer in which *RE* and Ta atoms order in trigonal antiprisms having different size (2.47(1) and 1.98(1)Å for the six *RE*-O1 and Ta2-O1 distances respectively), in agreement with the different radius of the rare earth and the transition metal ions. *RE* atoms shows two additional, slightly longer, interactions with O4 along the c axis, leading to a coordination polyhedron in form of a bi-capped trigonal antiprism. The ordered arrangement of the cations in the mixed *RE*-Ta layer implies interesting consequences from the spectroscopic point of view.

Table 2. Crystal data and structure refinement for $La_{0.95}Nd_{0.05}Ta_7O_{19}$.

Empirical formula	$La_{0.95}Nd_{0.05}Ta_7O_{19}$
Formula weight	1709.825
Temperature	293(2) K
Wavelength	0.71069 Å
Crystal system	hexagonal
Space group	$P\bar{6}c2$
Unit cell dimensions	a = 6.239(2) Å c = 20.003(6) Å
Volume	674.3(12) Å^3
Z	2
Density (calculated)	8.421 Mg/m^3
Absorption coefficient	59.77 mm^{-1}
F(000)	1440.3
Crystal size	0.12 x 0.05 x 0.03 mm^3
Theta range for data collection	2.01 to 27.50 deg.
Index ranges	$-8 \le h \le 7$, $-7 \le k \le 8$, $-25 \le l \le 25$
Reflections collected / independent	4686 / 537
Refinement method	Full-matrix least-squares on F^2
Data / restraints / parameters	537 / 0 / 31
Goodness-of-fit on F^2	1.293
Final R indices [I>2sigma(I)]	$R_1 = 0.0406$, $wR_2 = 0.1821$
R indices (all data)	$R_1 = 0.0476$, $wR_2 = 0.1821$
Extinction coefficient	0.0026(4)
Largest diff. peak and hole	4.05 and -3.07 e. Å^{-3}

Table 3. Atomic coordinates, displacement parameters ($Å^2$ x 10^4) and selected bond distances (Å) for $La_{0.95}Nd_{0.05}Ta_7O_{19}$ (Nd:LHT). For the anisotropically refined atoms, U_{eq} is defined as one third of the trace of the orthogonalized U_{ij} tensor. Occupancy factors for La and Nd on the RE site were fixed during the refinement at 0.95 and 0.05, respectively.

atom	x	y	z	$U_{iso/eq}$	U_{11}	U_{22}	U_{33}	U_{23}	U_{13}	U_{12}
Ta1	0.6412(2)	0.6398(2)	0.65624(3)	58(4)	94(9)	69(8)	29(6)	-4(2)	-3(2)	55(3)
Ta2	2/3	1/3	1/2	57(6)	72(7)	72(7)	28(8)	0	0	36(3)
RE	1/3	2/3	1/2	73(9)	89(12)	89(12)	41(14)	0	0	45(6)
O1	0.627(2)	0.571(2)	0.5566(6)	57(23)						
O2	0.013(4)	0.760(3)	0.6543(5)	87(23)						
O3	0.590(3)	0.631(3)	3/4	97(34)						
O4	1/3	2/3	0.638(13)	88(45)						
O5	2/3	1/3	0.667(11)	90(42)						

Ta1-O3	1.899(3)		
Ta1-O2	1.923(22)	Ta2-O1	6 x 1.978(11)
Ta1-O5	2.007(3)		
Ta1-O1	2.031(12)	RE-O1	6 x 2.466(10)
Ta1-O2	2.051(21)	RE-O4	2 x 2.656(26)
Ta1-O4	2.064(6)		
Ta1-O2	2.460(12)		

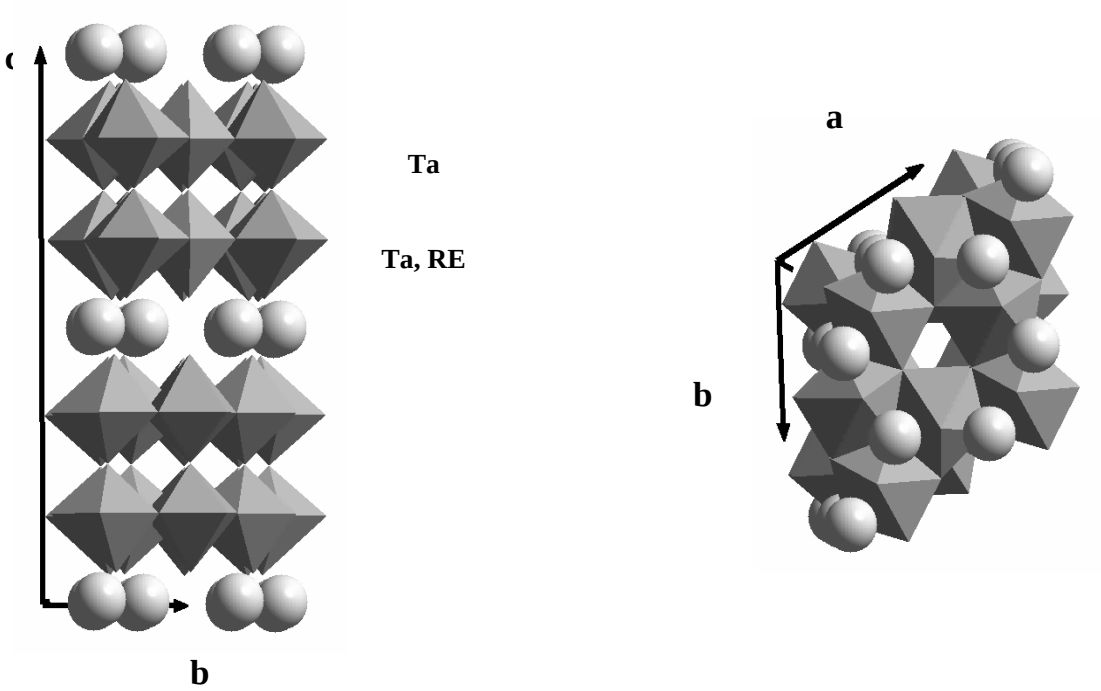

Fig. 3. Crystal structure of $RETa_7O_{19}$: (a) projection along the crystallographic a axis; (b) projection along the crystallographic c axis.

3.2 Spectroscopy

The energy level structure of Er^{3+} ion is shown on Fig. 5. To minimize cross-relaxation and up - conversion processes depopulating the upper laser level, the concentration of Er^{3+} should not exceed 1×10^{20} cm^{-3} [19].

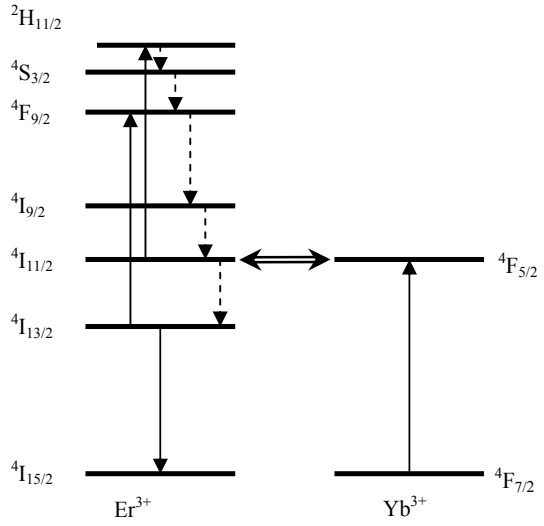

Fig. 4. Er^{3+}- and Yb^{3+}-ions energy-level scheme. Solid lines indicates absorption and emission transitions, dashed lines – nonradiative relaxation, double line – energy transfer.

A low concentration of erbium leads to low absorption of the pump radiation. This problem is usually solved by adding ytterbium ions. Yb^{3+} strongly absorbs pump radiation from laser diodes emitting around 980 nm and transfers it to the erbium ions thus considerably increasing the pumping efficiency. To decrease back-energy transfer to Yb^{3+} ions and reduce probability of excited state absorption to the level $^2H_{11/2}$ the lifetime of the $^4I_{11/2}$ level must be short (few μs). To fulfill this condition the non-radiative relaxation must dominate the de-excitation mechanisms of the $^4I_{11/2}$ level, which means that the phonon cut-off energy must be high in the crystal. And finally, the non-radiative relaxation and excited state absorption probability from the upper laser level $^4I_{13/2}$ should be negligible to get high laser efficiency.

Room-temperature polarized absorption spectra of (Er,Yb):YAB crystal in 980 nm spectral range are shown in Fig. 6. A strong absorption band corresponding to Yb^{3+} ions is centred at 976 nm in σ-polarization with maximal absorption cross-section of about 2.75×10^{-20} cm^2 and bandwidth of 17 nm (FWHM).

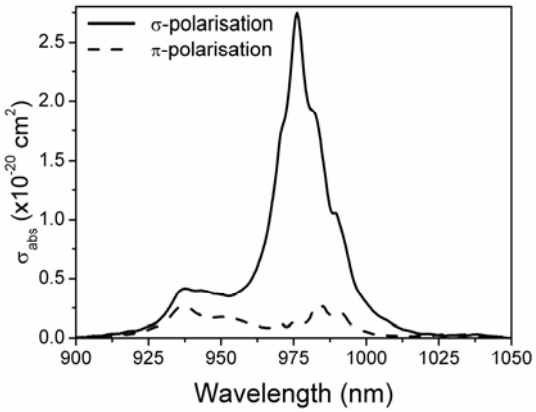

Fig. 5. Room-temperature polarized absorption spectra of (Er,Yb):YAB crystal in 1μm spectral range.

A number of local maxima are observed in the 1480-1605 spectral range of (Er,Yb):YAB absorption spectra in both polarizations. The strongest maximum with cross-section of about $3.8\cdot10^{-20}$ is located at 1530 nm in σ-polarization. The stimulated emission cross-section spectra shown in Fig. 7 were calculated using reciprocity method. The stimulated emission cross-section was estimated to be about $1\cdot10^{-20}$ cm^{-1} at 1602 nm for σ- and π-polarization.

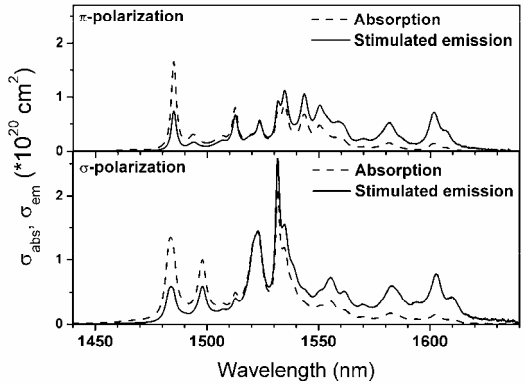

Fig. 6. Polarized absorption (solid line) and stimulated emission (dashed line) cross-section spectra of (Er,Yb):YAB crystal in 1.5 μm spectral range.

The luminescence decay time of the $^4I_{13/2}$ level of Er^{3+} was measured to be about 350 μs. The measured lifetime is significantly shorter than calculated from the Judd-Offelt analysis (4.41 ms [20]). Thus the luminescence quantum efficiency for the $^4I_{13/2}$ manifold of Er:YAB is about 8%.

Unfortunately, it was impossible to measure the luminescence decay of $^4I_{11/2}$ level of erbium directly because of the poor emission efficiency from this level. However, the absence of any upconverted green luminescence gives indirect evidence of short $^4I_{11/2}$ level lifetime (not more than a few microseconds).

Ytterbium $^2F_{5/2}$ level lifetime in Yb:YAB crystal was measured to be (480±5) μs, whereas the lifetime in co-doped Er,Yb:YAB is (60±5) μs. The shortening of the Yb^{3+} radiative lifetime in the erbium-ytterbium codoped crystal in comparison with ytterbium-doped one indicates strong non-radiative energy transfer from Yb to Er ions. The energy transfer efficiency was estimated to be about 88%.

The unpolarized 10 and 298 K absorption spectra of NHT, 5% Nd:LHT and 5% Nd:YHT are compared in Fig.8. The differences in the relative intensities reflect the differences in the activator concentrations. The observed multiplets have been assigned to the transitions from the $^4I_{9/2}$ ground state to the excited levels of the Nd^{3+} ion [21]. The components of these multiplets have full width at half maximum (FWHM) of the order of 10-15 cm^{-1}, a value typically observed in the case of ordered and good quality crystals. Their number sometimes exceeds that expected from the complete Stark splitting of the electronic levels of Nd^{3+}. In particular, in the spectra of Nd:LHT and Nd:YHT

a doublet occurs in the 430 nm region, where a single line is expected ($^2P_{1/2} \leftarrow {}^4I_{9/2}$ transition): this clearly indicates the presence of two non equivalent optical centers. The origin of these centers can be accounted for by supposing that the Nd^{3+} ions can enter not only the La (or Y) sites but also, to some extent the Ta1 or, less likely, the Ta2 sites of the host lattice.

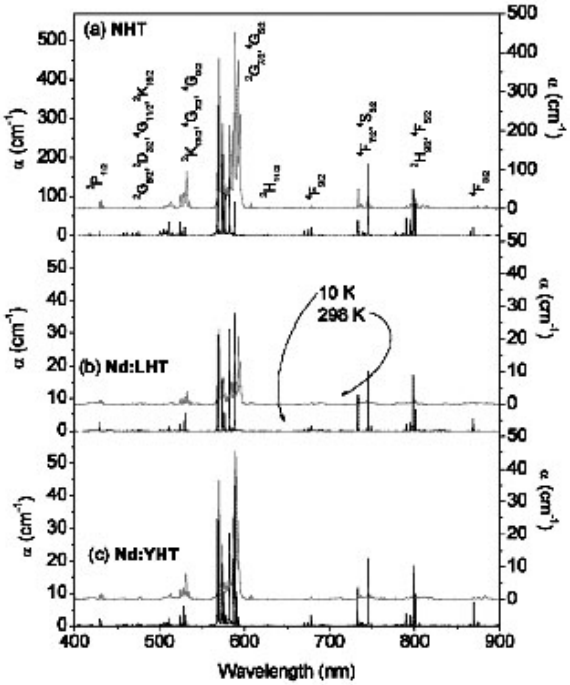

Fig. 7. 10 and 298 K absorption spectra of NHT (a), Nd:LHT (b) and Nd:YHT (c)

On passing from 10 to 298 K, the spectrum presents a number of 'hot' bands due to transitions originating from thermally populated Stark components of the ground state. Moreover, the optical features broaden up to FWHM values of about 30–40 cm^{-1} and give rise to broad bands attractive for diode pumping. The 10 and 298 K emission spectra (Fig. 9) are constituted of two manifolds located in the 880 and 1060 nm regions, and assigned to the transitions from the $^4F_{3/2}$ level to the $^4I_{9/2}$ and $^4I_{11/2}$ states, respectively. The 10 K spectra evidence the presence of two main and other minor optical centres, the latter probably constituted of Nd^{3+} located near to lattice defects. At room temperature the broadening of the emission features results in two broadband systems extending from 870 to 930 nm and from 1030 to 1100 nm, interesting in the perspective to develop tunable laser devices.

The emission decay curves of NHT and LHT and YHT doped with 1% and 5% Nd^{3+} have been measured as a function of the temperature. The observed profiles were single exponential, yielding decay times nearly independent of the temperature, as shown in the inset of Fig. 9. The decrease of their values with the concentration can be associated to energy transfer processes terminating in quenching centres. The relatively high decay time of NHT indicates that the efficiency of these processes is not very high. In our opinion, this is related to the fact that the interactions between the optical centres should be mostly confined within the RE, Ta layers, since the distance between two neodymium ions belonging to different layers cannot be shorter than 10 Å (Fig. 4*a*). This should significantly limit the efficiency of the energy transfer processes responsible of the concentration quenching of the Nd^{3+} luminescence.

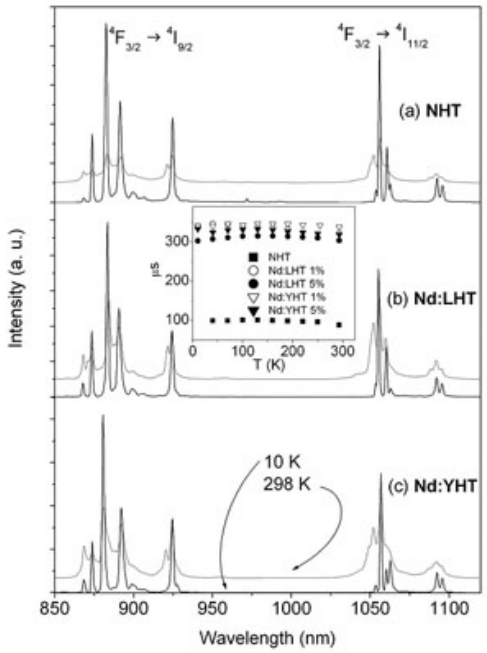

Fig. 8. 10 and 298 K emission spectra of NHT (a), Nd:LHT (b) and Nd:YHT (c). In the inset the temperature dependence of the decay times is reported.

3.3. Nonlinear and laser experiments

Input-output diagrams for Er(1at.%),Yb(11at.%):YAB CW laser are shown in Fig. 10. The maximal output power of about 245 mW with slope efficiency of 14% was obtained at 1604 nm for σ-polarization.

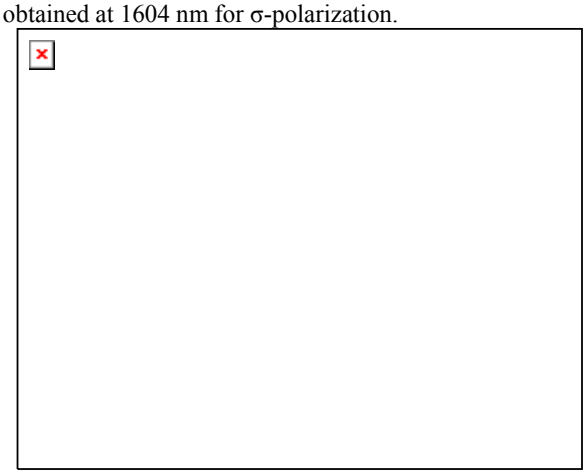

Fig. 9. Input-output diagrams of Er(1at.%),Yb(11at.%):YAB CW laser with output coupler transmittance of 0.8% (circles) and 1.5% (squares).

In the Q-switched mode with Co^{2+}:$MgAl_2O_4$ saturable absorber Er(1at.%),Yb (11at.%):YAB laser produced up to 108 mW of total output power with slope efficiency of 9.6% at 1604 nm (Fig. 11). The Q-switched pulse duration at maximal output power was about 135 ns with maximal pulse energy of 4.3 μJ.

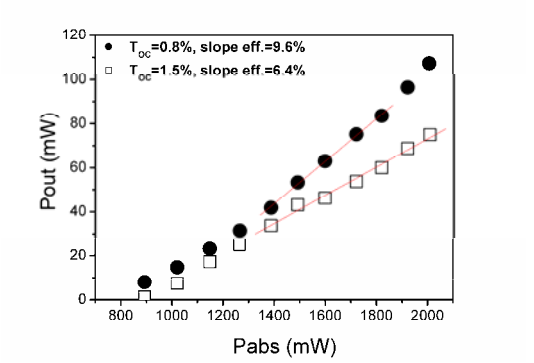

Fig. 10. Input-output diagram of the Q-switched Er(1at.%),Yb(11at.%):YAB laser with Co:MALO passive shatter with output coupler transmittance of 0.8% (circles) and 1.5% (squares).

In the case of borates such as Yb:YAB and Nd:YAB, Brazilian twins have been observed in the past using chemical etching followed by atomic force microscopy or optical microscopy (See for example [22]). In this case, the second harmonic generation has been measured across the crystal as a function of crystal orientation, but for some regions of the crystal face, the frequency conversion has unexpected double maxima as the crystal angle is tuned. This implies two or more twins are present in that region, and the second harmonic conversion efficiency is thus optimized for two different angles or orientations of the crystal. However, this "natural quasi-phase matching" does not improve the frequency conversion of the affected crystals.

The differential polishing /etching of the crystal exposes boundaries at the edges of the regions which also show the different frequency conversion performance, and these boundaries are consistent with the edges of twins. To clarify this phenomenon, a Yb:YAB crystal was cut into slices and each slice polished and again characterized. Boundaries were evident in Figs. 12*a* and 12*b* indicated by slight edges after polishing, which are consistent with the presence of twins. The edges of the region "a" in Fig. 12*a* are similar to those seen in Fig. 12*c*, which shows a second harmonic conversion map of the Yb:YAB crystal containing a central region with a single maximum of conversion efficiency and regions in the upper third which have maxima at other orientations corresponding to the presence of twins. Indeed, as the slices were traced through the crystal, the size of region "a" in Fig. 12*a* changed since the boundary of this twin was not perpendicular to the crystal faces. This crystal did not exhibit any evidence of refractive index variation using crossed polarizers or interferometry. Although its fundamental lasing performance was not spatially sensitive, its frequency doubling performance was extremely susceptible to position on the crystal, consistent with the twins present.

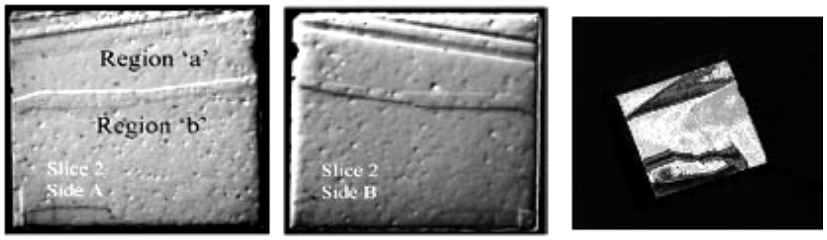

Fig. 11. Optical microscope images of two sides (A and B, Figs. 8a and 8b respectively) of a slice of the Yb:YAB crystal, after polishing, and its second harmonic conversion map (c).

Over 1.1W of green emission was obtained from a diode pumped Yb(8at.%):YAB crystal when the pumping power was 11W, and the conversion efficiency of diode-to green was 10% [3]. This is the maximum diode-pumped self-frequency-doubled (SFD) green output reported to date. High-beam-quality green and IR emission was attained due to good crystal quality and a lack of thermal problems. The maximum output for 1040 nm fundamental operation was 4.3W, with a slope efficiency of 48%. The green emission had a M^2 value of 1.6 or better, indicating that this self-frequency-doubled laser is extremely good at high pump powers.

CW single-longitudinal-mode output in the 1120-1140 nm range with a maximum infrared power of 23 mW, and SFD power of ~ 1 mW in the 560-570 nm region has been obtained in a coupled cavity Yb:YAB microchip laser with a plane-plane coupled-cavity resonator incorporating an 8% doped Yb: YAB crystal. The output ranged from 220 mW at 1064 nm with a slope efficiency of 22% and 6 mW of SFD green at 530 nm, to 22 mW at 1135 nm and ~ 1 mW SFD yellow at 568 nm obtained with a slightly different cavity [1].

4. Conclusions

New data on flux growth, composition, homogeneity, structural and physical characteristics *RE*:$YAl_3(BO_3)_4$ (RE = Yb, Er) and *RE*Ta_7O_{19} (*RE* = Y, Nd, La) crystals have been obtained. It was found that the average Er and Yb

segregation coefficients vary from 0.80 to 1.02, as a consequence of minor difference in the sizes of Y^{3+}, Er^{3+} and Yb^{3+} cations.

The results on the liquid phase epitaxy of Yb:YAB can be considered as the first stage towards development of these thin films for modern applications. A major problem which awaits clarification concerns controlled growth of these layers with optimal composition and thickness. Evaluation of the potential of rare earth doped YAB thin films for optical waveguides is in progress now.

A new method is proposed to characterize the nonlinear behavior of the borates and other active nonlinear laser crystals as a useful non-destructive technique. It avoids the need for chemical etching to identify crystal twins in particular samples, and, as it is quick to apply, it may be useful for characterization of new techniques to control crystal twins in active nonlinear crystals.

Polarized absorption and stimulated emission cross-section spectra of Er,Yb:YAB crystal were determined at room temperature. Lifetimes of Er and Yb ion levels and Yb→Er energy transfer efficiency were measured. The CW and Q-switched laser operations of this material under continuous-wave laser diode pumping at 980 nm was demonstrated. A CW output power of 245 mW with slope efficiency of 14% at 1604 nm was achieved. In the Q-switched regime an average output power of 108 mW with slope efficiency of 9.6%, repetition rate of 20 kHz and pulse duration of 135 ns was obtained. Over 1.1W of green emission was obtained from a diode pumped Yb:YAB laser.

Preliminary X-ray and optical spectroscopy measurements of RHT evidence a close relationship between the layered structure of these crystals and their absorption and emission properties, indicating that they are promising materials which deserve to be more thoroughly characterized in perspective of technological applications. Experiments are in progress in order to grow crystals having shape and size suitable for polarized light and stimulated emission measurements.

Acknowledgement

The authors thank Dr Peter Dekker for his many contributions to borate laser development. This research was supported by the grants of RFBR ## 04-05-64709, 05-05-08021 and 06-05-08103, RFBR&NSFC ## 04-05-39001,05-05-39003 and by grants of Russian President for young scientists MK-2794.2005.05, MK-4594.2006.05, MK-4456.2006.5

References

[1] P. A. Burns, J. M. Dawes, P. Dekker, J. A. Piper, J.Li, J.Y. Wang, Opt. Commun. **207** 315 (2002).

[2] N.I. Leonyuk, E.V. Koporulina, V.V. Maltsev, J. Li, H.J. Zhang, J.X. Zhang, J.Y. Wang, J. Cryst. Growth **277**, 252 (2005).

[3] P. Dekker, J.M. Dawes, J.A. Piper, Y. Liu, J. Wang Opt. Commun. **195**, 431 (2001).

[4] T. Schweizer, T. Jensen, E. Heumann, G. Huber, Opt. Commun. **118**, 557 (1995).

[5] B. Simondi-Teisseire, B. Viana, A.M. Lejus, J. M. Benitez, D. Vivien, C. Borel, R. Templier, C. Wyon, IEEE J. Quantum Electron. **QE-32**, 2004 (1996).

[6] H. Giesber, J. Ballato, G. Chumanov, J. Kolis, M. Deineka, J. Appl. Phys. **93**, 8987 (2003).

[7] I. Sokolska, E. Heumann, S. Kuck, T. Lukasiewicz, Appl. Phys. **B71**, 893 (2000).

[8] B. Denker, B. Galagan, L. Ivleva, V. Osiko, S. Sverchkov, I. Voronina, J.E. Hellstrom, G. Karlsson, F. Laurel, Appl. Phys. **B79**, 1287 (2000).

[9] N. I. Leonyuk, Prog.Cryst. Growth and Charact. **31,** 279 (1995).

[10] M. M.Chretien, D.Bodiot, Compt. Rend. **C263/2**, 882 (1966).

[11] I.N. Isupova, E. Ramon, E.P. Savchenko, E.K. Keler, Izv. Akad. Nauk SSSR, Ser. Neorgan. Materialy **11/2**, 384 (1975) (in Russian).

[12] F. A. Rozhdestvenskii, M.G. Zuev, A.A. Fotiev, VINITI, Dep. No 2346, Moskva, 13.06.1975 (in Russian).

[13] E. Cavalli, L.I. Leonyuk, N.I. Leonyuk, J. Cryst. Growth **244**, 67 (2001).

[14] E. Cavalli, E. A. Volkova, E. Bovero, G. Calestani, R. Ramponi, N. I. Leonyuk, J. Cryst. Growth, submitted.

[15] G. M. Sheldrick, SHELX-97. Program for the Refinement of Crystal Structures.(1997) University of Goettingen, Germany.

[16] P. Dekker, J. Dawes, Optics Express **12,** 5922 (2004).

[17] S.Yu. Stefanovich, Abstracts of papers. Eur. Conf. on Laser and Electo-Optics (CLEO–Europe 1994), Elsevier (1994) p. 249.

[18] F. Lutz, M.Leiss, J.Müller. J.Crystal growth. **47,** 130 (1979).

[19] W. You, Y. Lin, Y. Chen, Z. Luo, Y. Huang, Opt. Mater. (2006) (in press).

[20] D.J. Newman and B. Ng. Crystal Field Handbook (Cambridge University Press, 2000).

[21] B. Denker, B.Galagan, L.Ivleva, V.Osiko, S. Sverchkov, I.Voronina, J.E.Hellstrom, G.Karlsson, F.Laurel. Appl. Phys. B **79**, 1287 (2000).

[22] X. B. Hu, S.S. Jiang, W.J. Liu, C.Z. Ge, J.Y. Wang, H.F. Pan, C. Ferrari, S. Gennari, Nuovo Cimento D Condensed Matter **19D**, 175 (1997).

*Corresponding author: leon@geol.msu.ru